Sound Radiation Characteristics of Rectangular Duct: An Experimental Approach

Aswin P

A Thesis Submitted to

Indian Institute of Technology Hyderabad

In Partial Fulfillment of the Requirements for

The Degree of Master of Technology

भारतीय प्रौद्योगिकी संस्थान हैदराबाद
Indian Institute of Technology Hyderabad

Department of Mechanical Engineering

June 2014

Declaration

I declare that this written submission represents my ideas in my own words, and where ideas or words of others have been included, I have adequately cited and referenced the original sources. I also declare that I have adhered to all principles of academic honesty and integrity and have not misrepresented or fabricated or falsified any idea/data/fact/source in my submission. I understand that any violation of the above will be a cause for disciplinary action by the Institute and can also evoke penal action from the sources that have thus not been properly cited, or from whom proper permission has not been taken when needed.

(Signature)

ASWIN P

(Aswin P)

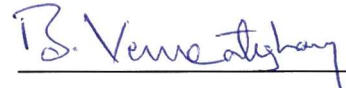ME12M1005

(Roll No.)

Approval Sheet

This Thesis entitled "Sound Radiation Characteristics of Rectangular Duct: An Experimental Approach" by Aswin P is approved for the degree of Master of Technology from IIT Hyderabad

(Dr B. Umashankar) Examiner
Dept. of Civil Engineering
IITH

(Dr Prashanth Kumar R.) Examiner
Dept. of Mechanical and Aerospace Engineering
IITH

(Dr B. Venkatesham) Adviser
Dept. of Mechanical and Aerospace Engineering
IITH

(Dr B. Umashankar) Chairman
Dept. of Civil Engineering
IITH

Acknowledgements

First and foremost I would like to thank my thesis guide Dr B. Venkatesham for his valuable support and guidance to improve the work throughout its course and allowing me to conserve my individuality. Next I would like to thank Dr B. Umashankar and Dr Prashanth Kumar R. for their constructive critiscism during thesis evaluations. I extend my sincere thanks to workshop in-charge Mr.Satyanarayan and every workshop personnel, especially Mr.Brahmachari, Mr.Madhu, Mr. Praveen Mr.Ashok, Mr.Jagadishan and Mr.Kiran Kumar for the related work and their readiness to help. Also, I am very grateful to my labmates and friends in IITH who gave wonderful life insights.

Dedication

"To all those who conserves curiosity towards nature's magic"

Abstract

The sound radiation characteristics of rectangular duct depend on acoustical and structural subsystems response. The coupling of acoustic duct modes and structural duct wall modes plays a critical role in generating noise in transverse direction of the duct, and its called as break-out noise. For finding coupled behaviour of the system, uncoupled analysis of each subsystem is necessary. Experimental modal analysis (EMA) of a standard dimension rectangular duct specimen is the first practical step. It helps to understand the coupling behavior between acoustic and structural modes in HVAC ducts. As an initial study of EMA, we found the Modal Assurance Criteria (MAC) for fixed-free beam, free-free and fixed-free conditions of rectangular steel plate and free-free conditions of rectangular duct. Finally, for simply supported rectangular duct, modal parameters have obtained using Experimental Modal Analysis (EMA). Correlated EMA results with Finite-Element Analysis (FEA) results using MAC method. An acoustic source for providing plane waves to the rectangular duct have been set up and found the input sound power supplied to the duct cavity. Methodology to find input sound power have been introduced. Using the assistance of various experimental techniques, we found the sound power radiated from the duct walls and compared.

Contents

Chapter 1

Introduction

1.1 Motivation

HVAC(Heating, Ventilating, Air-conditioning systems) comprises of ductlines of various geometries, mainly circular, flat-oval and rectangular. The latter one serves as our matter of concern here. Air ducts are responsible for providing fresh, heated or
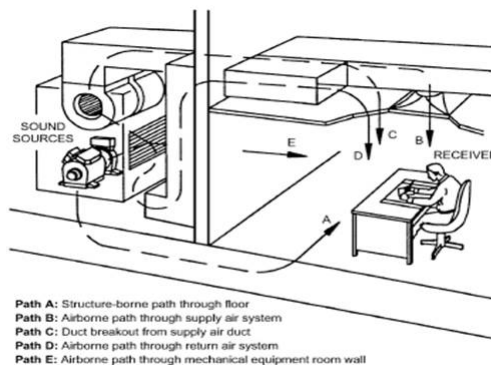
Figure 1.1: Different paths through which sound escapes to reach receiver

cool air for the building ensuring a pleasant climate for its inhabitants. There are some undesirable side effects associated with it which causes noise generation and transmission to the occupant's space. Main noise sources of such systems are fans, blowers and break-in noise. The air-borne noise transmitted through the duct reaches the living space through the supply and return air systems. This problem can be resolved to great extent by lining the interior of the duct with suitable sound absorbing material or airduct silencers. In addition to the air-borne noise from the duct outlets, sound can also be transmitted directly through the walls of the duct into the occupied

space. This is called breakout noise. As shown in the Fig. 1.1, the path C kind of noise generation is our subject of interest.

1.2   Literature Survey

Towards the end of 1970s, the studies related to break-out noise from the HVAC ducts made of thin shells have started. For predicting the transmission loss, various models have been introduced. Among these, Cummings[1] started his work by assuming that a rectangular duct radiates sound in the same way as a finite-length line source incorporating a single travelling wave. He further modelled as finite-length cylindrical radiator[2]. The cross section geometry highly influences the breakout characteristics. The three most common cross sectional duct shapes are circular, flat-oval and rectangular. There is a change in the pattern of transmission loss of the ductwork with respect to its cross sectional geometry. A rectangular duct cross section has low breakout wall transmission loss at low frequencies because of the strong structural response to the internal sound field. The circular cross-section ducts have a very high transmission loss at low frequencies. The ducts with flat oval cross sections can be expected to display the transmission loss characteristics of both, the rectangular and the circular duct cross-section [3]. There lies the importance of predicting methods for transmission loss of rectangular flexible ducts.

On the other side, an advantage of break-out noise is, it results in natural noise attenuation as the ductline is considerably lengthy. Obviously, it is not applicable in noise-sensitive areas. Thus it serves as a way of reducing noise level in unlined ducts. Also studis shows that by the use of lined ducts, noises above frquencies 850 Hz can be eliminated.

Venkatesham et al [4] put forward the equivalent plate model representation of the rectangular duct. In this, rectangular duct has been unfolded into an equivalent plate where creases are replaced by linear springs and joint is replaced with combination of rotational and linear springs. Also acoustic pressure and vibration velocity are expressed in terms of uncoupled acoustic and structural sub systems. The analytical solution provided is in good agreement with the numerical results.

It has been shown [5] that modes of natural vibration of a box-type structure can be classified into six groups according to the symmetry properties of the three panel pairs forming the box. At frequencies well below the critical frequency of the plates of the box, it is found that the sound radiation directivity of each box mode can be correlated to that of elementary sound sources like monopole, dipole etc. The radia-

tion efficiency of all box modes reaches a peak at critical frequencies, and above that, gradually approaches unity.

NASA Langley Research Center[6] empirically calculated joint rotation constants for different joint types in rocket launch vehicles which are basically cylindrical bodies. Joints have been classified into loose, moderate, good and excellent for the empirical studies. Also, the results of the studies of the effects of looseness in interstage connections, the unsymmetric behaviour of a supposedly symmetrical structure, nonlinear characteristics are discussed.

Conventionally, we use contact type excitations such as impact hammer as well as using shaker to extract modal parameters. But the use of non-contact type excitations like internal and external sound sources is new to the area of experimental modal analysis (EMA). The advantage of non-contact type excitations over contact type excitations for experimental modal analysis has been discussed by Farshidianfar et al. [7]. Mainly closely coupled modes or pseudo-repeated modes at higher frequncies can be effectively captured.

Statistical Energy Analysis (SEA) can be used as an efficient analytical tool to predict transmission losses, especially at higher frequencies. Because numerical tools like FEM and BEM fails at higher frequencies. But below 200-400 Hz, where modal density is usually lower, this method is very inaccurate. Since it deals with averaged response over a frequency range, it can't predict the mode shapes of the system.

Modal Assurance Criterion (MAC) is a statistical indicator, used in our work for correlating mode shapes acquired from Numrical Modal Analysis (NMA) to that of EMA. Reference[8] reviews the using of the Modal Assurance Criterion. The MAC is most sensitive to large differences and relatively insensitive to small differences in the mode shapes. This inturn makes it as a good statistic indicator and gives a good correlation between mode shapes.

In this work we have tried to establish experimental techniques to measure the breakout noise. Experimental Modal Analysis (EMA) has been applied to extract modal parameters of the structure. Experimental rig has been setup in order to conduct these tests. The two extreme cases of sound field in the duct cavity are anechoic field and reverberent field. Out of this, we have chosen reverberent sound field inside duct cavity for different tests.

1.3 Outline of Thesis

NMA results and EMA results has been compared with each other and changes have been incorporated as an attempt to effectively duplicate the experimental duct's dynamic behaviour using numerical modelling.
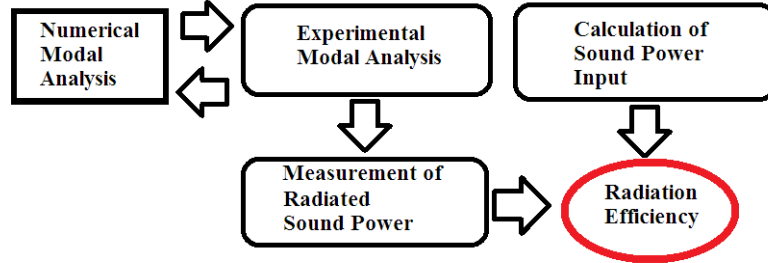

Figure 1.2: Schematic diagram to depict the experimental approach to find the radiation efficiency

As evident from the flowchart (fig. 1.2), our final objective was to obtain the sound radiation efficiencies, through experimental techniques. Sound power input calculation for the experimental was required. Also, particle velocity measurement system has been implemented to measure sound radiation from the duct walls.

Chapter 2 explains the analytical metod and experimental technique to find sound power input from the cylindrical duct.

Chapter 3 covers comparison of EMA and NMA of various structures including rectangular duct.

Chapter 4 describes experimental calculation of sound power radiation of rectangular duct.

Chapter 5 concludes the thesis work.

Chapter 2

Sound Power Input Calculation

2.1   Directivity of Sound Source

For conducting the sound power radiation measurement of the rectangular duct, we have to substitute an appropriate noise source for reconstructing the noise inside duct. Thus a speaker delivering sound energy through a cyindrical duct to the rectangular duct has been selected. The cylindrical duct (refer fig. 2.1) serves as a system to form plane acoustic waves. The fig. 2.1 demonstrates the experimental details for measur-
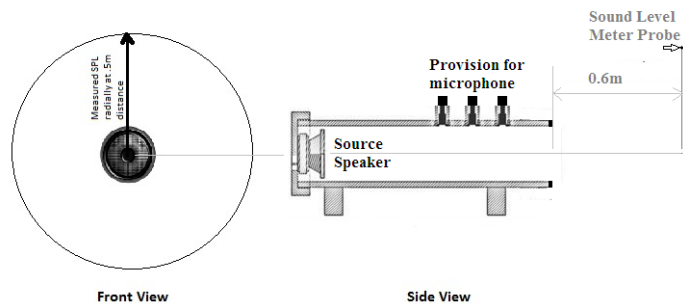

Figure 2.1: Measuring directivity of sound source

ing directivity of the sound source. The experiment is intended to give directional characteristics of the source in a plane parallel to the cross-section of the cylinder. Measurements have been taken using B&K Sound Level Meter, at 13 locations at an equal interval of 30deg, for four different input sound signals. Since our frequency range of interest lies between 20Hz to 400Hz, pink noise, 100 Hz sine wave, 250 Hz sine wave and 500 Hz sine wave has been chosen as input signals. Polar Direcivity curves (see fig. 2.2) corresponding to those four signals have been obtained.
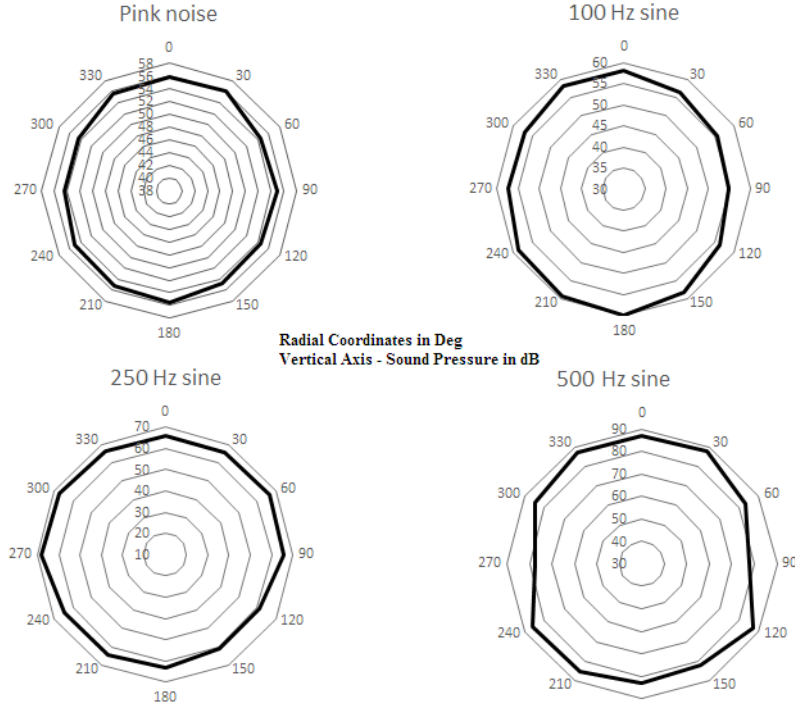
Figure 2.2: Polar Directivity of Speaker-Cylindrical tube arrangement

Here, as we give higher frequency signals the isoclinic curve is getting unsymmetrical. Meaning, higher the input signal frequency we give, the symmetric nature of the source directivity is reducing. But as our interested range of frequency is low, plane wave acoustic excitation can be obtained.

2.2 Determining Sound Power Input

Sound power input supplied to the rectangular duct has to be quantified as the first step towards determining sound radiation efficiencies. The Sound Power delivered W_{in}, to the duct cavity is given by the below equation,

$$W_{in} = \frac{S_{AA}}{2\rho c} A_s \tag{2.1}$$

where S_{AA} is the autospectrum of the progressing pressure wave and A_S is the cross-sectional area of cylindrical interior. In fig. 2.3 shown, A represents the progressive pressure wave and B represents the reflecting pressure wave. Measure the pressure signals at location 1 and 2, using two microphones.
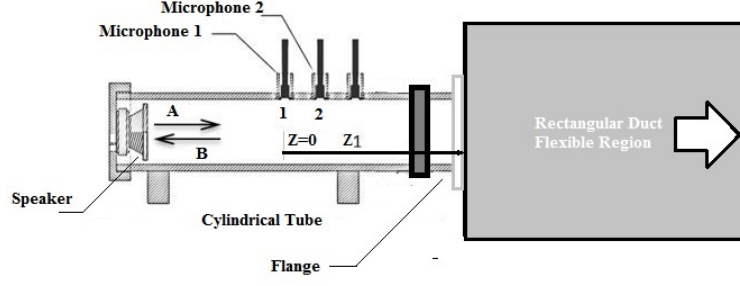
6

Figure 2.3: Sound Power Input Measurement Set Up

2.2.1 Calculating Autospectrum

As discussed above, we have to obtain S_{AA}. At any location inside the cylindrical tube, the total pressure p(z, t) is given by (refrence from [9])

$$p(z,t) = A(f)e^{j(\omega t - kz)} + B(f)e^{j(\omega t + kz)} \qquad (2.2)$$

where k is the wave number and z is the distance from position 1.
So,

$$p(0,t) = (A(f) + B(f))e^{j\omega t} \qquad (2.3)$$

The above equation after Fourier Transform over finite time T is

$$P_1(f,T) = A(f,T)e^{-jkz_1} + B(f,T)e^{jkz_1} \qquad (2.4)$$

$$P_2(f,T) = A(f,T)e^{-jkz_2} + B(f,T)e^{jkz_2} \qquad (2.5)$$

If S_{AA}(f) and S_{BB}(f) are autospectral densities of A(f) and B(f), respectively, and C_{AB} and Q_{AB} are real and imaginary parts of S_{AB}(f), crossspectral density between A(f) and B(f), then

$$S_{11}(f) = \frac{1}{T}\{P_1(f,T)P_1^*(f,T)\} \qquad (2.6)$$

$$S_{11}(f) = S_{AA}(f) + S_{BB}(f) + 2\{C_{AB}(f)cos(2kz_1) + Q_{AB}(f)sin(2kz_1)\} \qquad (2.7)$$

$$S_{22}(f) = \frac{1}{T}\{P_2(f,T)P_2^*(f,T)\} \qquad (2.8)$$

$$S_{22}(f) = S_{AA}(f) + S_{BB}(f) + 2\{C_{AB}(f)cos(2kz_2) + Q_{AB}(f)sin(2kz_2)\} \qquad (2.9)$$

$$C_{12}(f) = Re[S_{12}(f)] = Re[\frac{1}{T}\{P_1(f,T)P_2^*(f,T)\}] \tag{2.10}$$

$$C_{12}(f) = S_{AA}(f)cos(k(z_1 - z_2)) + S_{BB}(f)cosk((z_1 - z_2)) + \tag{2.11}$$

$$C_{AB}(f)[2cos(k(z_1 + z_2))] + Q_{AB}(f)[2sin(k(z_1 + z_2))] \tag{2.12}$$

$$Q_{12}(f) = Im[S_{12}(f)] = Im[\frac{1}{T}\{P_1(f,T)P_2^*(f,T)\}] \tag{2.13}$$

$$Q_{12}(f) = -S_{AA}(f)sin(k(z_1 - z_2)) + S_{BB}(f)sin(k(z_1 - z_2)) \tag{2.14}$$

By solving the above equations(2.7-2.13), we have the expression for S_{AA} as

$$S_{AA} = \frac{1}{4}cosec(kz)^2[S_{11} + S_{22} - 2C_{12}cos(kz) + 2Q_{12}sin(kz)] \tag{2.15}$$

Therefore, to obtain S_{AA} experimentally, we have to acquire autospectral densities of pressure signals at position 1 and 2, S_{11} and S_{22} respectively, and the cross-spectrum betweem pressure signals at position 1 and 2.

2.2.2 Sound Power Input Results

We measured S_{11}, S_{22} and S_{12}, for random noise as input signal. The interested frequency range is 27.8-1000 Hz. The distance of microphone 2 from microphone 1 is 0.224m. The sound power input in dB for $1/3^{rd}$ octave band frquencies is as shown in fig. 2.4.
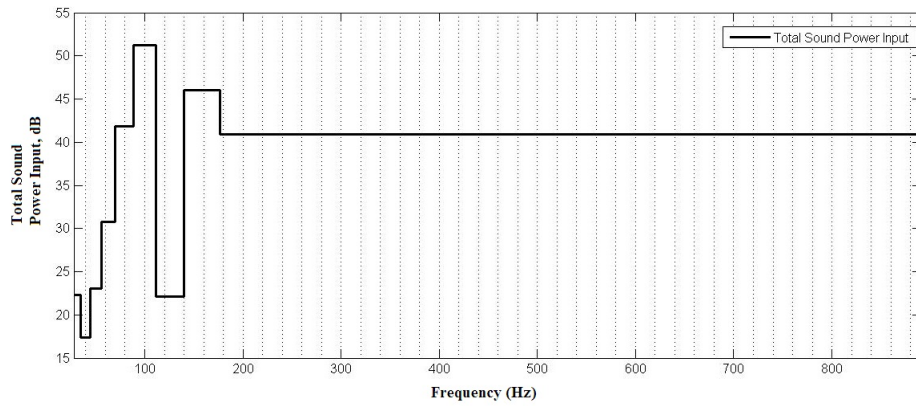

Figure 2.4: Total sound input power(dB)

Chapter 3

Modal Analysis

3.1 Numerical Modal Analysis

Numerical Modal Analysis can be conducted as a prior study for Experimental Modal Analysis. The commercial software ANSYS was chosen as a tool for numerical modal analysis. This comparison process will give an idea regarding the number of dofs and the reference position of the accelerometer to be chosen while conducting EMA. EMA analysis of cantilever beam, rectangular plate have been conducted before rectangular duct EMA study.

3.1.1 Cantilever Beam

A beam with dimensions 3.5cm×0.35cm×39cm is chosen for EMA. Material properties of Steel is applied. Cantilever boundary conditions are used in the numerical study.
Shell63 element type is used for numerical modelling. Number of elements in it was 276.

3.1.2 Rectangular Plate (free-free)

A steel rectangular plate with dimensions of 40 cm length, 29.6 cm width and 0.3 cm thickness has been considered for NMA study. The material of steel considered has density 7800 kg/m^3, Young's modulus 210 GPa, and Poisson's ratio 0.3. Rectangular plate was meshed with elements of shell 63, and number of elements are 76. Free-Free boundary conditions have applied.

3.1.3 Rectangular Plate (fixed-free)

Steel rectangular plate with dimensions of 30 cm length, 29.6 cm width and 0.3 cm thickness has been considered for NMA study. The material properties are density 7800 kg/m^3, Young's modulus 210 GPa, and Poisson's ratio 0.3. Rectangular plate meshed with elements of shell 63, and number of elements of 67. Free - Free boundary conditions have applied.

3.1.4 Rectangular Duct (free-free)

Rectangular Duct consists three parts (see fig. 3.1). They are

- Flexible Region: This constitute the main duct part having a length of 1.2m and 1.01mm thickness.
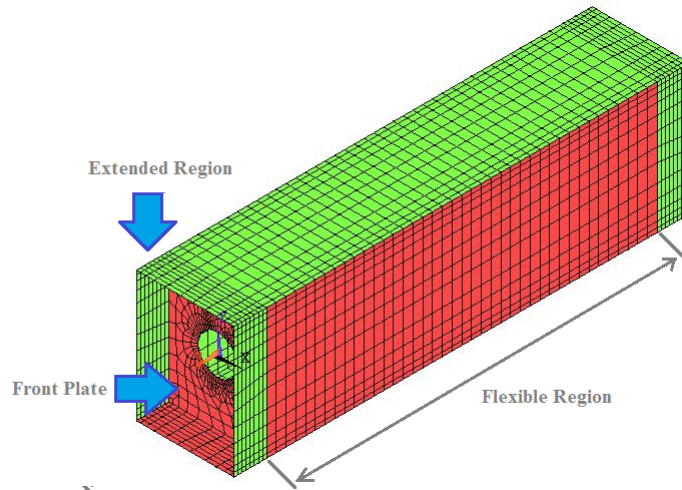

Figure 3.1: Numerical Model of Rectangular Duct

- Extended Wall: Extended from flexible region inorder to apply boundary condition for EMA. But thickness is 1.5mm, higher than flexible portion, to make sure that it won't disturb the vibration study of former portion.

- End plates, front and back: Again for the study of the experimental coupled analysis, reverberating sound field has to be established inside flexible region. Front plate has a center hole of 122mm dia, to mount the speaker. Both plates has 40cm height, 30cm width and a thickness of 3.5mm.

Material properties of G.I steel having density 7800 kg/m^3, Young's modulus 210 GPa, and Poisson's ratio 0.3. Rectangular duct was meshed with elements of shell 63, and number of elements are 4109. Free-Free boundary conditions have applied.

3.1.5   Reactangular Duct (Simply Supported)

Rectangular duct with free-free boundary conditions as discussed in previous section has been modified for simple supported boundary conditions. It is the major objective of current work to understand the structural-acoustic coupled phenomena. The simply
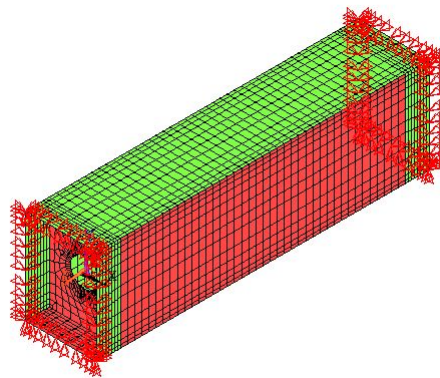

Figure 3.2: Numerical Meshed Model of Rectangular Duct with simply supported boundary conditions.

supported boundary conditions are given along the extreme edge lines as shown in fig. 3.2.

3.2   Experimental Modal Analysis (EMA)

The objective of conducting experimental modal analysis is to experimentally find the modes and corresponding frequencies which characterize the dynamic behavior of the structure. These quantities subsequently can be used to corroborate numerical model by comparing the numerical modeshapes and frequencies with the experimental modeshapes and frequencies. This section describes the experimental test procedure and the curve fitting methods to determine the different mode shapes of different structures.

3.2.1 Excitation System

The input excitation for EMA is given by any of these excitation systems like impact hammer, shaker, step relaxation and self-operating. If we preload the structure and suddenly remove the load, the excitation is called step relaxation. Self-operating involves exciting the structure through an actual operating load. Obviously, as the input cannot be measured in most of the cases, this method is not popular. Shaker testing and impact testing are the popular ones. Excitation systems can also be classified as attached as well as non-attached, e.g. shaker and impact hammer respectively. The modal parameter extraction using acoustic excitation is also an existing technique. Here we have chosen impact hammer to excite the structure in EMA. If the hammer is moving and accelerometer is fixed, it is called as roving hammer method.

For exciting the structure, the selection of hammer tip is important. Generally there are soft, hard and medium hammer tips which can be of rubber, steel and plastic material, respectively. If we have to excite at wide range of excitation hard tip has to be used. Softer tip is best when frequency range of interest is narrow.

3.2.2 SIMO and MIMO

There are two different classifications for any EMA based on the number of excitation inputs and response channels or locations. MIMO (Multiple Input Multiple Output) is one classification, where multiple shakers are used for excitation and multiple responses are acquired. SIMO (Single Input Multiple Output) is the other, which would use one excitation system and multiple response locations. We have used SIMO for EMA.

3.2.3 Windowing and Leakage

Two common time domain windows that are used in impact testing are the force and exponential windows(ref.[10]). After sampling the signal, these windows are applied, even before the application of FFT. In time domain, any non-zero data following the impulse signal in the sampling window is considered to be measurement noise. The force window selects the impulse signal alone and removes the noise lying away from the impulse signal.

To reduce leakage in the response spectrum, exponential window is applied to the impulse signal. The FFT process the impulse signal assuming it to periodic in the transform window, which is the data samples collected. To be periodic in the trans-

form window, the waveform must have no discontinuities at its beginning or end. To consider as a periodic signal in transform window, (i) The signal should completely appear in the transform window (ii) The cyclic signals should be present in integer number of cycles.

Obviously, it may not be always possible for the time signal to be periodic in the data samples collected and smearing of its spectrum takes place, which is called leakage. Spectrum distortion and inaccuracy of the data are the problems caused by the leakage. In short, if the response signal in an impact test diminishes to zero before the end of the sampling window, there will be no leakage, and hence no need of any window. On the other hand, if the response does not decay to zero before the end of the sampling window, an exponential window must be used to reduce the leakage effects in the response spectrum. The exponential window adds artificial damping to all of the modes of the structure in a known manner. After curve fitting, this added component will be deducted from the estimated modal damping. Thus the exponential window is very important as it prevents leakage or makes it minimum, resulting in the capturing of impulse window from the tranform window.

3.2.4 Frequency Response Function

Frequency Response Function(FRF) can be defined here as the ratio of output in frequency domain to the input in frequency domain. Assumes linearity, time invariance, observability, and reciprocity when we calculate FRFs estimation. FRF is a complex quantity. Therefore it can be expressed as any of the following

- Real part of FRF vs Frequency

- Imaginary part of FRF vs Frequency

- Magnitude of FRF vs Frequency

- Phase of FRF vs Frequency

Refer fig. 3.3 and fig. 3.4 for pictorial explanations. A driving point measurement is a measurement where the input degree of freedom (DOF) is the same as the output DOF. The imaginary part of a driving point FRF should be completely positive or completely negative, depending on the positive or negative orientation of the input and output signals. The peaks or dips of the imaginary part of a driving point FRF correspond to the system resonances.The phase is 90^0 during resonance and imaginary part becomes maximum as real part tends to zero.
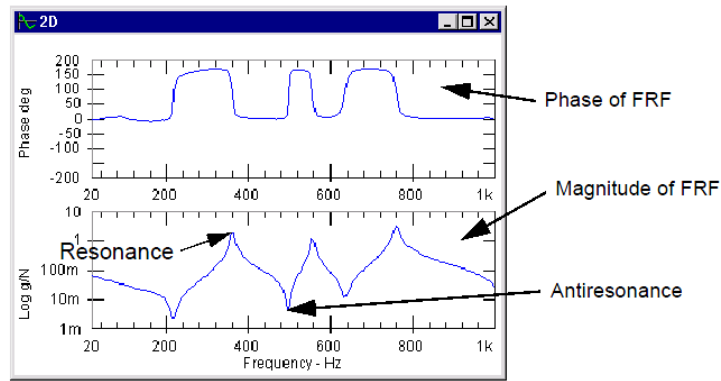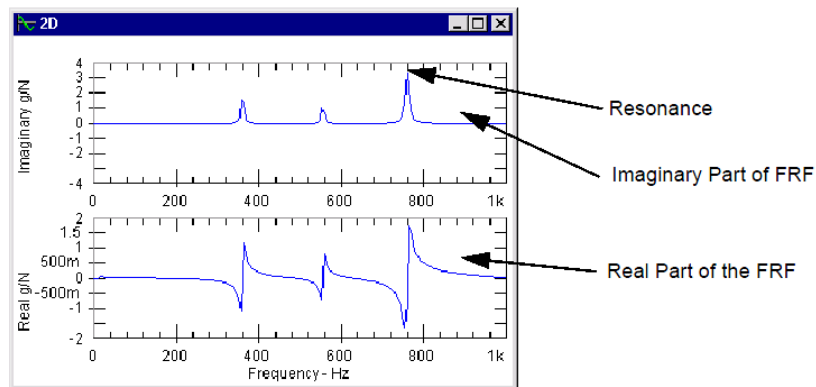
Figure 3.3: Phase and Magnitude of FRF

Figure 3.4: Real and Imaginary parts of FRF

3.2.5 Coherence

Coherence describes the assumption of linear system. Its an averaged function of autopowers and crosspowers. Any noise source that results in a response not linearly related to the input causes incoherence.Coherence ranges from 0 to 1. But ideally it should be closer to 1. Coherence value will improve with good Signal to Noise ratio value. It can be improved by increasing number of measurements for averaging.

3.2.6 Closely spaced modes and pseudo-repeated modes

In the FRF plot, if two modal frequencies are closely lying then there will be a common frf associated with them. The associated mode shape will be the summation of those two modes. If the structure is symmetric, two different mode shapes can appear at the same frequency called the pseudo-repeated modes, but their mode shapes are different.

14

3.2.7 Curve-fitting Algorithms

Experimental modal parameters are estimated by applying curve fitting to a set of frequency response functions (FRFs). The outcome of curve fitting is a set of modal parameters for each mode that is identified in the frequency band of the FRF measurements. The unknown parameters of the parametric form are the modal frequency, damping and residue for each mode.

All curve fitting methods fall into one of the following categories,

- Local SDOF

- Local MDOF

- Global

- Multi-Reference (Poly Reference)

In general, the methods are listed in order of increasing complexity. SDOF is short for a Single Degree of Freedom, or single mode method. Similarly, MDOF is short for a Multiple Degree of Freedom, or multiple mode method. SDOF methods estimate modal parameters one mode at a time. MDOF, Global, and Multi-Reference methods can simultaneously estimate modal parameters for two or more modes at a time. Local methods are applied to one FRF at a time. Global and Multi-Reference methods are applied to an entire set of FRFs at once. Local SDOF methods are the easiest to use, and should be used whenever possible. SDOF methods can be applied to most FRF data sets with light modal density (coupling). MDOF methods must be used in cases of high modal density.

Global methods work much better than MDOF methods for cases with local modes. Multi-Reference methods can find repeated roots (very closely coupled modes) where the other methods cannot. From (displacement/force) or (acceleration/force) FRFs, the peak values of the imaginary part of the FRFs are taken as components of the mode shape. This is called the Quadrature method of curve fitting. From (velocity/force) FRFs, the peak values of the real part are used as mode shape components. Hence, using the simplest Local SDOF curve fitting methods, all three modal parameters (frequency, damping, and mode shape) can be extracted directly from a set of FRF measurements.

There are three different mode indicators; the modal peak function, the complex mode indicator function (CMIF) and the multivariate mode indicator function (MMIF). Any of the mode indicators can be used to count peaks from a set of single reference

FRFs. The CMIF and MMIF indicators provide more information from a multiple reference set of FRFs. The complex mode indicator function (CMIF) performs a singular value decomposition of the FRF data, resulting in a set of multiple frequency domain curves. The number of mode indicator curves equals the number of references. Each peak in a curve is an indication of a resonance. The multivariate mode indicator function (MMIF) performs an energy minimization of either the real or imaginary part of the FRF data, resulting in a set of mode indicator curves. Like CMIF, the number of curves equals the number of references, and each peak in a curve is an indication of a resonance.

3.2.8 EMA on different structures

Based upon the guidance given by the NMA, EMA conducted on the same structures given in the section 3.1. Before conducting the EMA using roving hammer method and tri-axial acclerometer, geometry information defined by the nodes and elements, has given as the input in the wireframe model. Therefore the number of DOF's are established for the EMA of each structure.

3.2.9 Cantilever beam

Wireframe model of beam consists of 14 nodes as shown in fig. 3.5. Fixed-free condi-
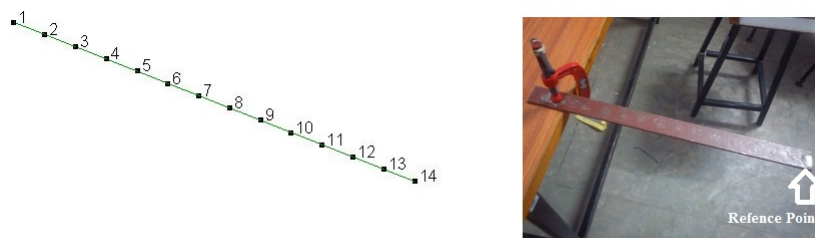
Figure 3.5: Wireframe model of cantilever beam and experimental set up

tion has been given by the c-clamp at one end and other end leaving free. For exciting we choose steel tip since we need wide range of frequencies. We applied quadrature method of SDOF for finding mode shapes.

3.2.10 Rectangular Plate(free - free)

Wireframe model of plate consists of 45 nodes as in fig. 3.6. Free-free condition has been given by placing the plate on a soft material. For exciting we choose steel tip
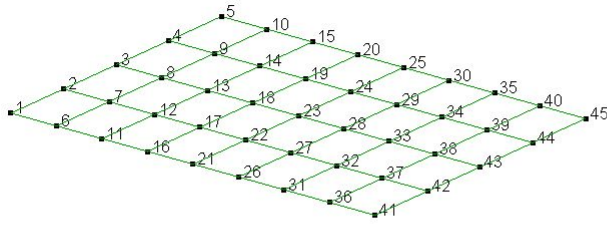
Figure 3.6: Wireframe model of rectangular plate and experimental set up

since we need wide range of frequencies. We applied quadrature method of SDOF for finding mode shapes.

3.2.11 Rectangular Plate(fixed - free)

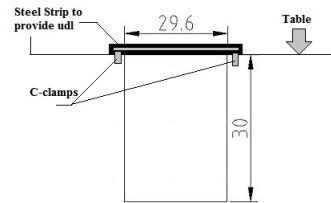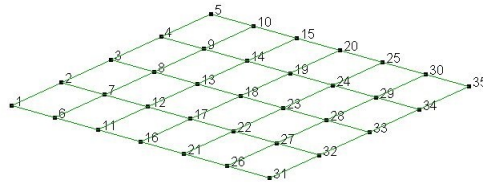Wireframe model of plate consists of 35 nodes as shown in fig. 3.7. Fixed-free condition

Figure 3.7: Wireframe model of rectangular plate and experimental set up

has been given by the arrangement of steel strip with C-clamps. All procedures same as in free-free EMA of the plate.

3.2.12 Rectangular Duct(free - free)

Rectangular duct had been made using G.I steel and duct joint is of Pittsburgh lock (fig. 3.8). Wireframe model of this duct consists of 144 nodes as in fig. 3.9. The duct has been hanged using bungee rope inorder to give approximate free-free boundary condition. Since it has high modal density, we used MDOF algorithm to extract modal parameters. Also MMIF was the mode indicator function chosen, shown in fig.

3.10. Tri-axial acclerometer was used to capture flexural modes. After selection of number of dips in MMIF, next stage in postprocessing is producing synthesized FRF by tracking the stable poles, given by diamond symbol. Hence it is called stabilty diagram, as shown in fig. 3.11.

3.2.13 Rectangular Duct(Simply supported)

Rectangular duct had been subjected to simply supported condition using fixtures as shown in fig. 3.12(picture ref.[11]) and fig. 3.13.

The steel balls attached to the end frames give the point contact and hence prevent the normal motion of the duct walls. The end frames are further carried by the hook kind of fixture. Further, the pre-processing, geometry and post-processing was similar to the EMA for free-free duct.

3.3 Modal Assurance Criterion (MAC)

MAC is a statistical indicator used to correlate mode shapes obtained from NMA to those from EMA. It is a simple technique and does not require an estimate of the system matrices. MAC values lies within 0 to 1. MAC with 1 indicates exact resemblance with each other. If it is 0 then modeshapes doesn't have any match. Also it doesn't compares frequencies.

$$MAC_{ij} = \frac{|\{V_i^{EMA}\}\{V_j^{NMA}\}|^2}{\{\{V_i^{EMA}\}\{V_i^{EMA}\}\}\{\{V_j^{NMA}\}\{V_j^{NMA}\}\}} \tag{3.1}$$

Eq.(3.1) gives the expression for calculating MAC, where
V_i^{EMA} and V_j^{NMA} are the modal vectors from EMA and NMA, respectively. MAC can best represented as a matrix colour plot as in shown in fig. 3.14

3.4 Comparison of results from NMA (FEM) and EMA

3.4.1 Cantilever Beam

For cantilever beam, both mode shapes as well as modal frequencies of EMA and NAM were matching reasonably well(see fig. 3.16 and fig. 3.15).
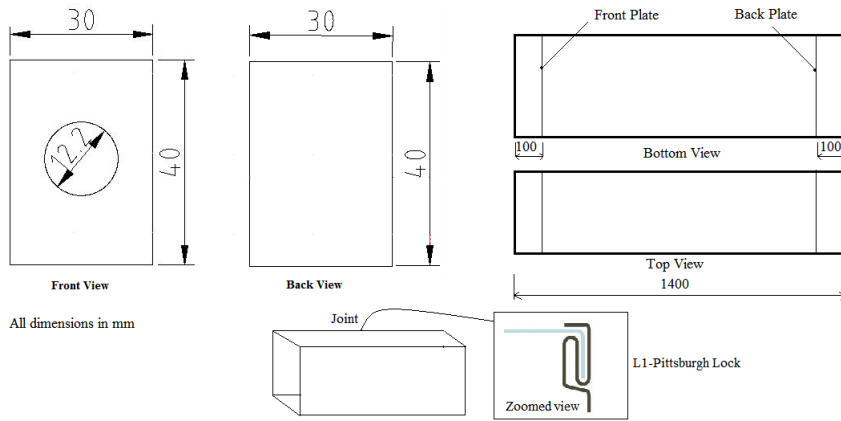
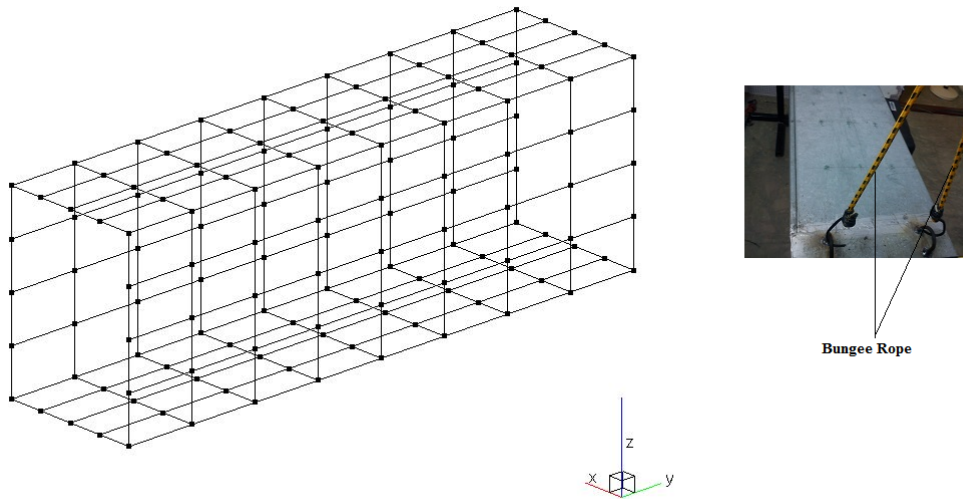Figure 3.8: Dimensional details of the duct and joint type

Figure 3.9: Wireframe model of rectangular duct and experimental set up
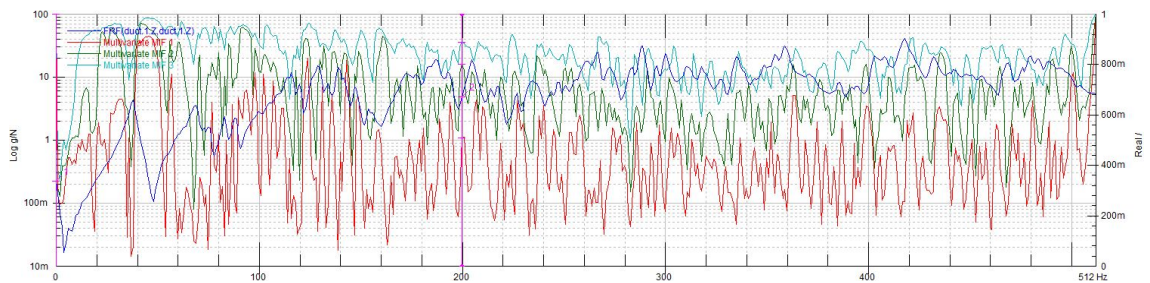

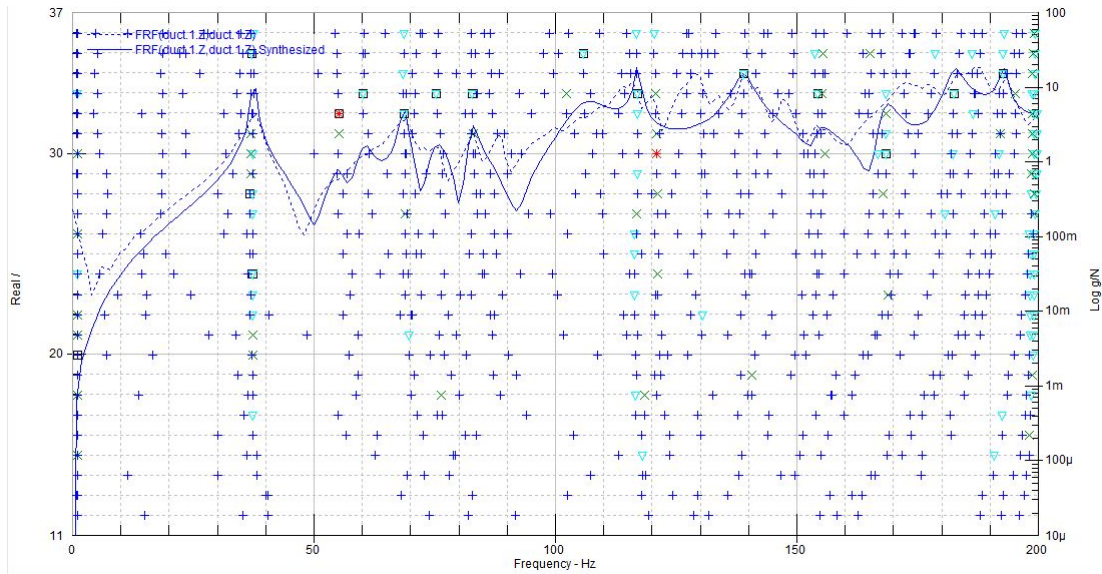Figure 3.10: Multivariate Mode Indicator Function and selection of dips

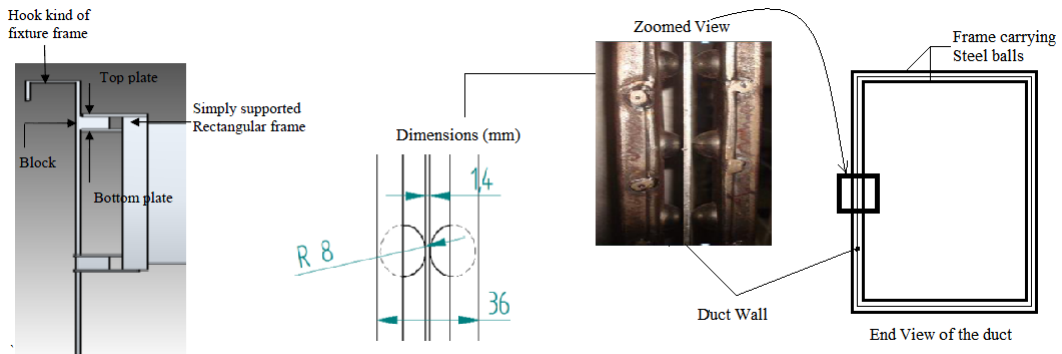Figure 3.11: Stability Diagram and synthesised FRF

Figure 3.12: Detailed view of Simply supported condition and fixture assembly, Ref.[11]

Mode 3 has not been captured because we used uni-axial accelerometr which cannot handle lateral DOF. Again in EMA, we modelled cantilever beam as line element, hence fifth mode is also missing. MAC values for other modes are above 0.9.

3.4.2   Rectangular Plate (free - free)

Now for the EMA of the rectangular plate(free- free) best correlation(see fig. 3.17 and fig. 3.18) has been achieved between NMA and EMA results, as a result of changing accelerometer from uni-axial to tri-axial.

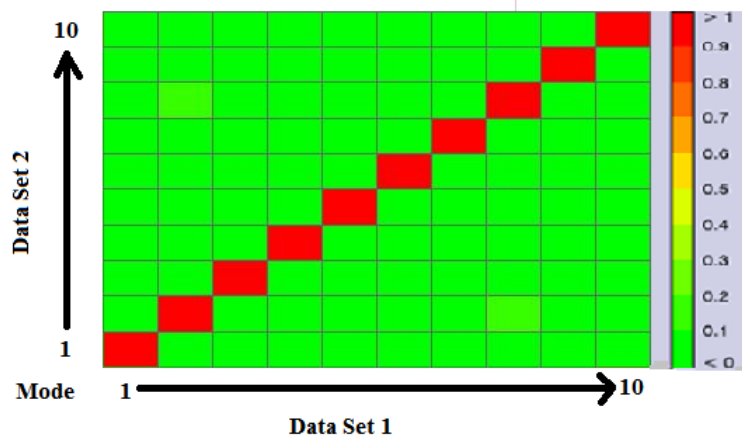Figure 3.13: Rectangular duct(SS) for EMA set up
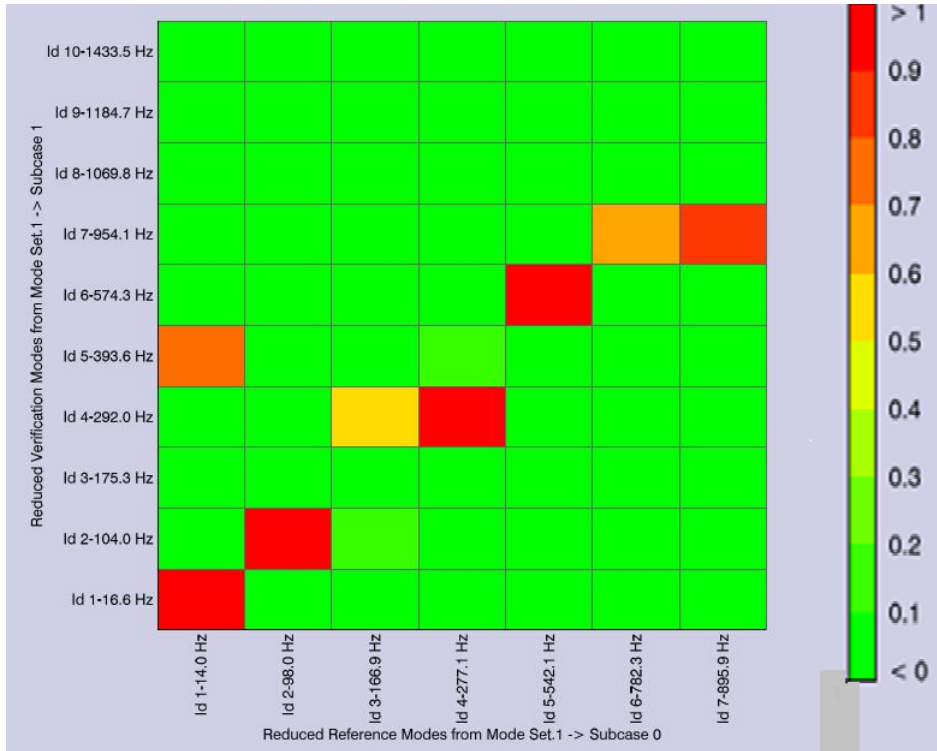

Figure 3.14: MAC colour plot

Figure 3.15: MAC colour plot of Cantilever beam

3.4.3 Rectangular Plate(fixed - free)

By introducing a boundary condition(fixed-free) to the same free-free plate we discussed above, results is shown in fig. 3.20 and fig. 3.19 have been observed. It is clear from these comparatively lower MAC values that boundary constraints can bring more uncertainty to the numerical model. Tri-axial couldn't capture lateral motion efficiently, hence first mode is missing in EMA result. Also, the fourth mode is absent as reference point was on a node location.
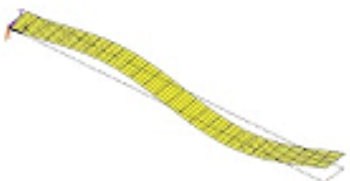
Sr. No.	Natural frequency (Hz)		EMA	FEM
	EMA	FEM		
1	14.0	16.6		
2	98.0	104.0		
3	-	175		
4	277.1	292.0		
5	-	393.3		

Figure 3.16: Comparison of Modal Parameters from EMA and NMA

23
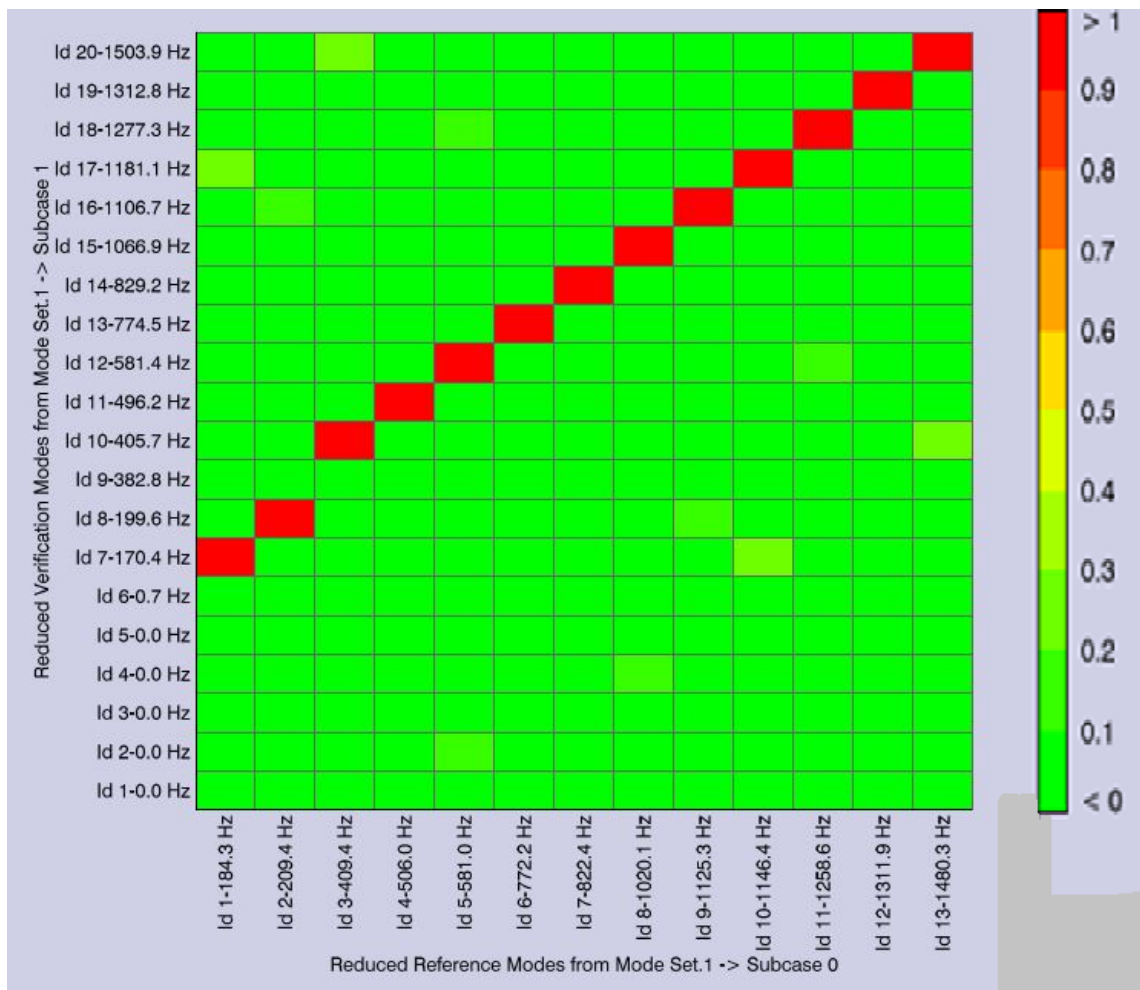
Figure 3.17: MAC colour plot of free-free Plate

Mode No.	Natural frequency (Hz)		Mode Shape	
	EMA	FEM	EMA	FEM
1	184.3	170.4		
2	209.4	199.6		
3	409.4	405.7		
4	506.0	496.2		
10	1146	1181.1		

Figure 3.18: Comparison of Modal Parameters from EMA and NMA of free-free plate

Figure 3.19: MAC colour plot of fixed-free Plate
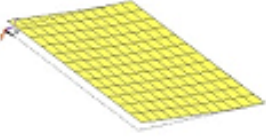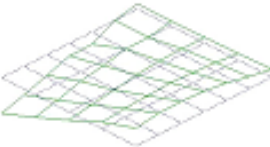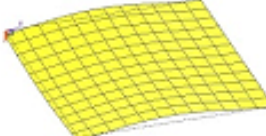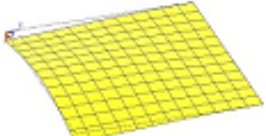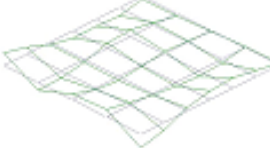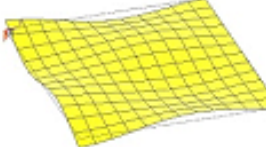
Mode No.	Natural frequency (Hz)		Mode Shape	
	EMA	FEM	EMA	FEM
1	——	57.7	——	
2	131.3	142.9		
3	324.5	354.5		
4	——	461.32	——	
10	1464	1571.8		

Figure 3.20: Comparison of Modal Parameters from EMA and NMA of fixed-free plate

3.4.4 Rectangular Duct (free - free)
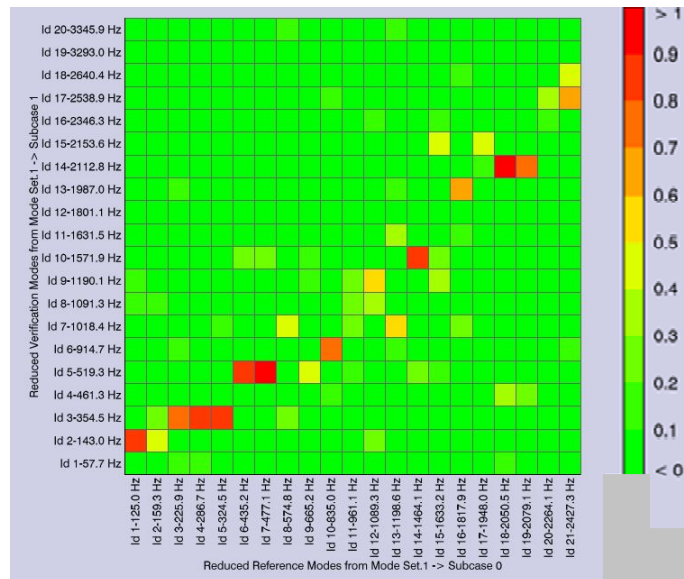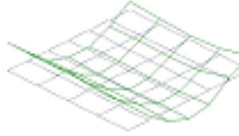
From NMA, using ANSYS, for rectangular duct(free-free), we found the modal density was too high,(refer table 3.1). Therefore, modal parameter estimation from impact

Table 3.1: Modal frequencies obtained from NMA for free-free rectangular duct

Mode	Freq(Hz)(NMA)	Mode	Freq(Hz)(NMA)	Mode	Freq(Hz)(NMA)
1	0	11	38.035	21	67.887
2	0	12	42.248	22	69.146
3	3.01E-04	13	43.512	23	70.763
4	0.10946	14	47.574	24	74.599
5	0.12469	15	51.558	25	77.908
6	0.27341	16	52.452	26	78.678
7	21.746	17	54.603	27	81.214
8	28.011	18	56.538	28	82.136
9	30.067	19	56.603	29	85.383
10	33.607	20	63.932	30	89.659

Table 3.2: Modal frequencies obtained from EMA for free-free rectangular duct

Mode	Freq(Hz)	Mode	Freq(Hz)
1	37.6	6	72.8
2	39.5	7	103.5
3	58.9	8	115.3
4	67.6	9	150.7
5	68.5	10	283.7

method becomes too difficult.

To conduct coupled analysis, atleast modes till 150 Hz has to be determined with minimum error.

Because, the first coupling frequency is appearing around 140 Hz, obtained using numerical simulation[11]. But the failure to capture fundamental mode in EMA is still a question. The figure 3.21 shows the fundemental mode shape in all the three directions. MAC values are not consistent for all modes, as evident from fig. 3.22. Table 3.3 shows the data for modes with comparatively higher MAC values and similar modal frequencies.
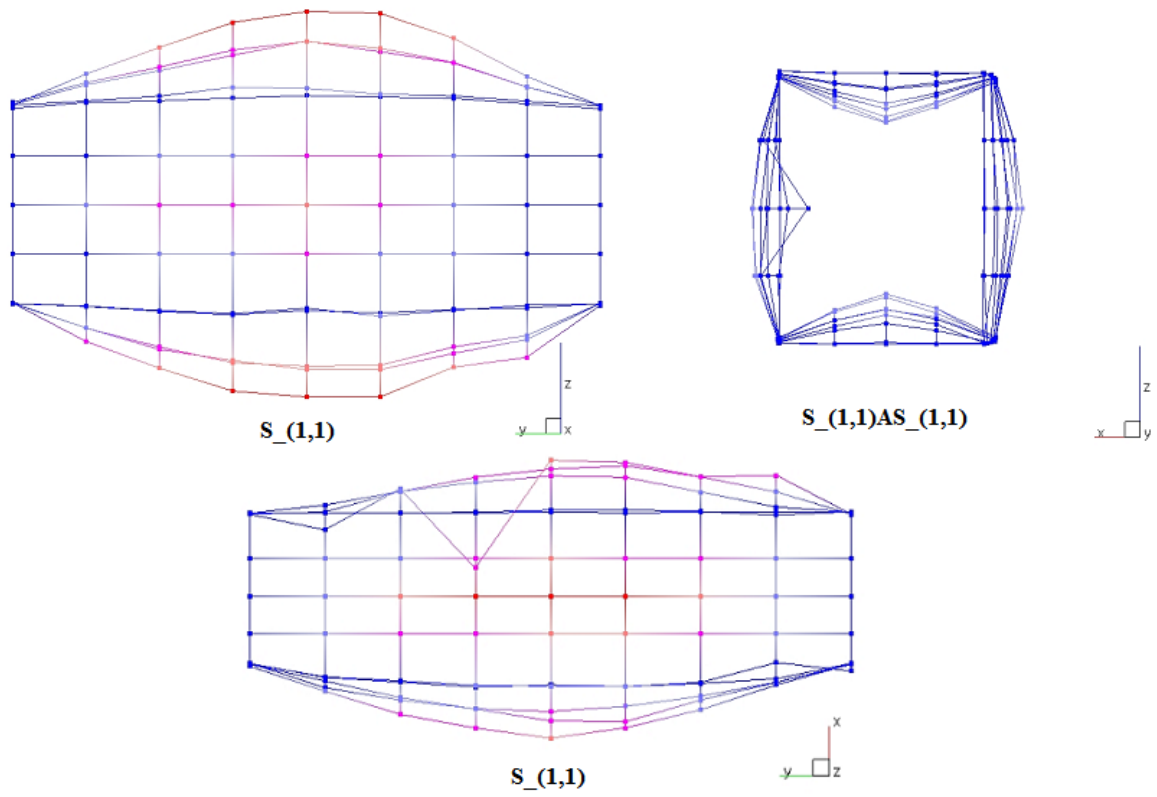
Figure 3.21: Mode Shapes in X, Y and Z directions at fundemental frequency 35.87Hz

Table 3.3: MAC table for free-free rectangular duct

Mode No.	Freq(Hz)EMA	Mode No.	Freq(Hz)NMA	MAC value	Δ Freq
1	37.6	9	30	0.846	-7.56
3	58.9	18	56.6	0.686	-2.3
4	67.6	14	47.6	0.542	-20.05
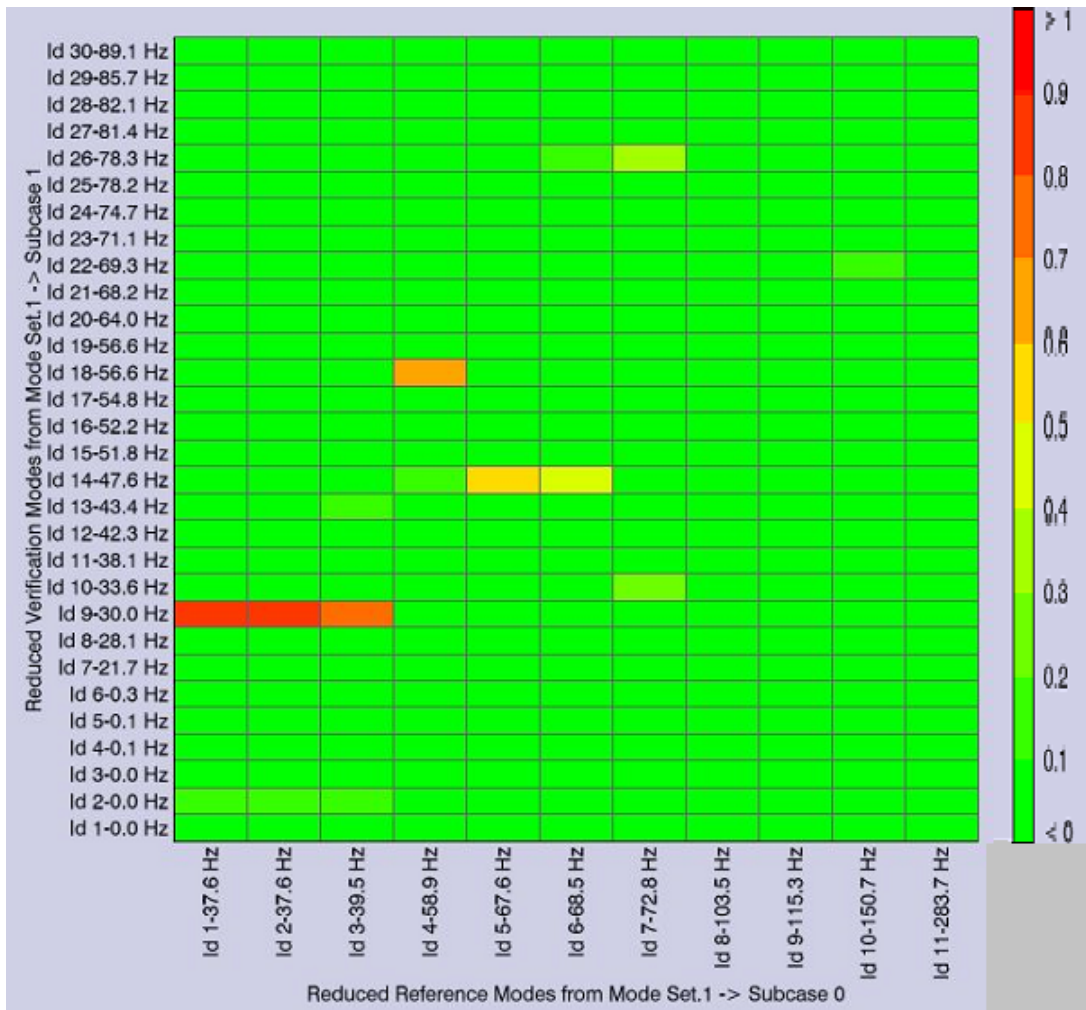
Figure 3.22: MAC colour plot of free-free rectangular duct

3.4.5   Rectangular Duct(S-S)

As expected the MAC values became poorer, because of the application of boundary constraints. Again the experimental modal frequencies are also deviating than the acceptable limits from the numerical model. Figure 3.23 shows the mode shapes at fundemental frequency obtained from EMA. From Table 3.4, the modal density is
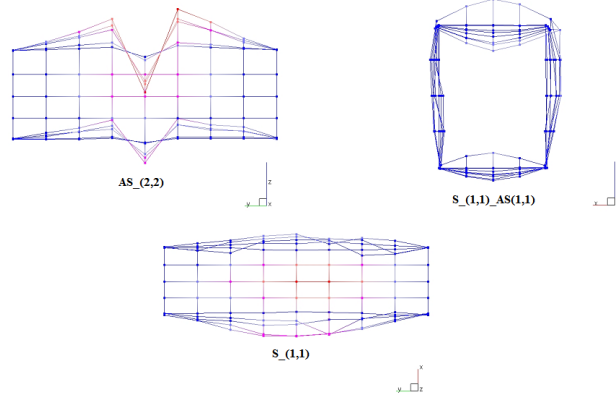
Figure 3.23: Mode shape of recatangular duct(S-S) at fundemental frequency 36.8 Hz from EMA

found to be high, as 40th mode is appearing at 128.84Hz. Also as there is simply supported boundary condition, MAC values have found to be reduced compared to the free - free boundary condition, as shown in Table 3.5.

Table 3.4: Modal frequencies obtained from NMA for S-S rectangular duct

Mode	Freq(Hz)	Mode	Freq(Hz)
1	21.757	7	41.869
2	28.024	8	47.027
3	28.056	9	51.816
4	33.062	10	52.463
5	38.15	11	54.539
6	41.524	40	128.84

Table 3.5: MAC table for S-S rectangular duct

Mode No.	Freq(Hz)EMA	Mode No.	Freq(Hz)NMA	MAC value	Δ Freq
1	36.8	2	28	0.44	-8.8
5	60.3	13	56.6	0.672	-3.67
6	63.6	13	56.6	0.67	-6.94

3.5 Modification in existing models

For rectangular duct, both free-free and simply supported cases, initial exprimental results were not in good agreement with NMA. Modal density was too high which made it cumbersome to extract modal parameters through impactor method. But eventhough there was a curiousity to obtain atleast their fundemental mode as well as to improve the existing MAC values.

As a result the following modification have been made and analysed the results.

- In the numerical model we modified the corners of the rectangular cross-section by applying fillet radius of 2mm(see fig. 3.24) to make the model closer to the exprimental duct. But the results showed that negligible difference it had with respect to the previous model results.

Fillet Radius 2mm applied at corners
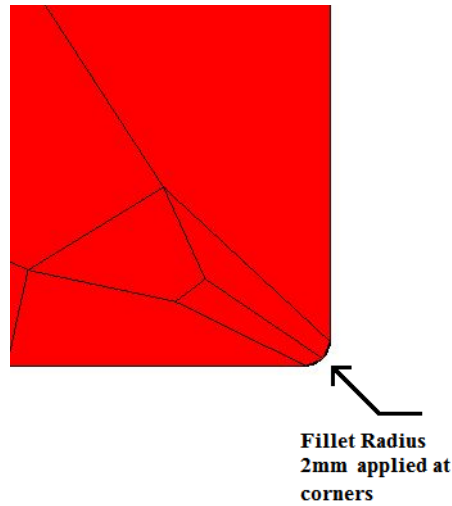
Figure 3.24: Fillet radius of 2mm applied at the edges (zoomed view)

- Initially, we considered only the flexible region of the duct for EMA. Therefore this time we included the extended wall as well as the end plates in EMA (see results in Table 3.6). But results were a little worser than earlier.

Table 3.6: MAC table for free-free rectangular duct considering end plates and extended wall in EMA

Mode No.	Freq(Hz)EMA	Mode No.	Freq(Hz)NMA	MAC value	Δ Freq
1	37.8	9	30	0.835	-7.76
2	39.6	13	43.5	0.214	3.88
4	68.4	14	47.6	0.345	-20.85

- Finally, in numerical model, based on the assumption that all edges of the duct are having higher rotational stiffness than expected, we have given the rot Z d.o.f equal to zero for all edges within the flexible region. As a result fundamental modal frequencies of both NMA and EMA came closer whereas MAC values stayed same, in simply supported and free-free mode of rectangular duct(see Tables 3.7 and 3.8).

- As a new EMA technique, acoustic excitation using pink noise was given. Using accelerometer, accelerations have been plotted for a section of duct. Frequencies captured using peak picking method, are shown in Table 3.9. This technique proved to capture some modes that has not found in impact method. But modal density is closer to impact method.

Table 3.7: MAC table after imposing zero rotZ for edges in NMA(free-free rectangular duct)

Mode No.	Freq(Hz)EMA	Mode No.	Freq(Hz)NMA	MAC value	Δ Freq
1	37.6	2	37.1	0.818	-0.43
4	67.6	12	68.5	0.473	0.86
5	68.5	12	68.5	0.438	0.02

Table 3.8: MAC table after imposing zero rotZ for edges in NMA(S-S rectangular duct)

Mode No.	Freq(Hz)EMA	Mode No.	Freq(Hz)NMA	MAC value	Δ Freq
1	36.8	2	37.1	0.436	0.31
2	37.2	2	37.1	0.412	-0.08
5	60.3	11	68.5	0.55	8.2
6	63.6	11	68.5	0.552	4.93

Table 3.9: Modal Frequencies with acoustic excitation

Mode No.	Freq (Hz)	Mode No.	Freq (Hz)
1	23.4	8	82
2	33.7	9	98.1
3	36.6	10	105.5
4	48.3	11	115.7
5	52.7	12	134.8
6	64.5	13	146.5
7	68.8	14	152.3

Chapter 4

Sound Power Radiation

Sound Power is the cause which produces the effect called sound pressure in a medium.Inorder to determine the sound power using systems like pp-probes, a control surface is defined. Thus the total sound energy radiated from the surface is measured in a direction normal to the surface. Sound Intensity is the sound power per unit area, and can also expressed as

$$\vec{I} = <I(t)>_T = <p\vec{u}> = \frac{1}{T}\int_0^T p\vec{u}dt \qquad (4.1)$$

where
p is the instantaneous pressure and u is the particle velocity.
Thus it is the time averaged rate at which work is done by the elements of fluid on their adjacent elements moving through unit area.
In order to obtain sound power we have to seek intensity measurement techniques. In far-field pressure and particle velocity are in-phase, so intensity is a real quatity. In near-field, both exists in out of phase, therefore intensity exists as complex quantity, as active intensity and reactive intesity. Active part is the propagating energy, known as acoustic intensity. Reactive part consists of evanascent energy, which diminishes rapidly as we move away from the source. Sound intensity can be measured in virtually any environment.On-site measurements can be handled well. By using sound intensity measurements on a control surface as described above, the sound power of a given noise source can be determined even in the presence of other radiating sources. The intensity measurement techniques mainly consists of intensity measuring probes, PP and PU types.

4.1 PP-Intensity Probe

The PP probe is consists of two matched microphones separated by a spacer for measuring sound pressure and estimates particle velocity from the pressure gradient. The following mathematical equation describes the intensity measurement using PP-intesity probe.

$$\hat{I}_r = <\hat{p}\hat{u}_r>_t = \langle \frac{p_1(t) + p_2(t)}{2} \int_{-\alpha}^{T} \frac{p_1(\tau) - p_2(\tau)d\tau}{\rho\Delta r} \rangle_t \tag{4.2}$$

where the caret $\wedge$ indicates an estimated quantity, t indicates averaging over time, ρ is the density of air, and r is the microphone separation distance. Limitations that are unavoidable with this technique are due to the finite difference approximation, scattering and diffraction, the size of the probe and instrumentation phase mismatch.

4.2 PU-Intensity Probe

A p-u sound intensity measurement system combines two fundamentally different transducers, one for measuring pressure using microphone and other for measuring particle velocity using microflown based technique. The Microflown sensor working principle uses two extremely sensitive heated platinum wires because of their feeble thermal resistance (Refer fig. 4.1[12]). In an environment of air flow, the heat transfer of the upstream wire occur and the heat will be carried away to the downstream. Thus the downstream wire is not allowed for effective heat transfer. Due to this, downstream wire will be at a bit higher temperature than upstream wire. Thus, a sensor voltage is generated which is linearly proportional to this temperature gradient between the wires, shown in fig. 4.2[12]

The sound intensity is simply the time average of the instantaneous product of the pressure and particle velocity signal,

$$I_r = \langle pu_r \rangle_T = \frac{1}{2}Re\{pu_r^*\} \tag{4.3}$$

Here we are acquiring both pressure and particle velocity signals through different sensors simultaneously. Such systems are sensitive to reactive sound fields. Reactivity is defind as the ratio of reactive intensity to the active intensity in log scale. Especially in near fields, if the reactivity takes a high value, then even a very small phase mismatch error between the two transducers gives rise to a considerable bias error,
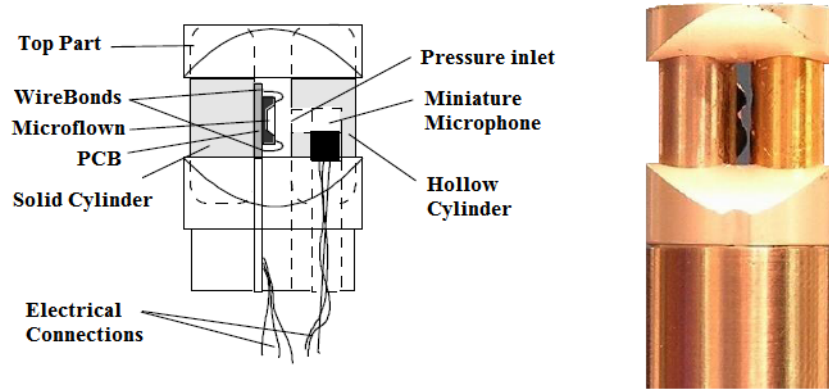
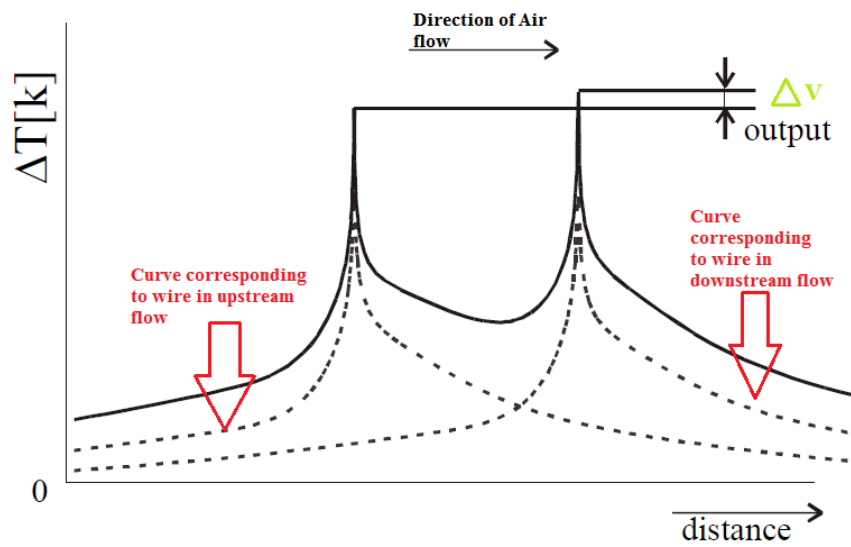Figure 4.1: Microflown probe details, interior and exterior view[12]

Figure 4.2: Microflown probe working principle[12]

as evident from the below expression:

$$\hat{I}_r = I_r(1 - \phi_e tg\phi_{field}) \tag{4.4}$$

where
$\hat{I}_r$ is the measured intesity, ϕ_e is a small phase error between measured and actual particle velocity, ϕ_{field} is the phase shift of the sound field, I_r is the true intensity.

4.3   Experimental Results

4.3.1   PU probe versus Accelerometer Measurements

Before introducing PU probe for measuring sound radiation from duct walls, consistency of PU probe compared to accelerometer data have tested. It has been found that displacement data obtained using PU probe is in good agreement with accelerometer data, as shown in fig. 4.3. Although the color plot or relative displacement data was
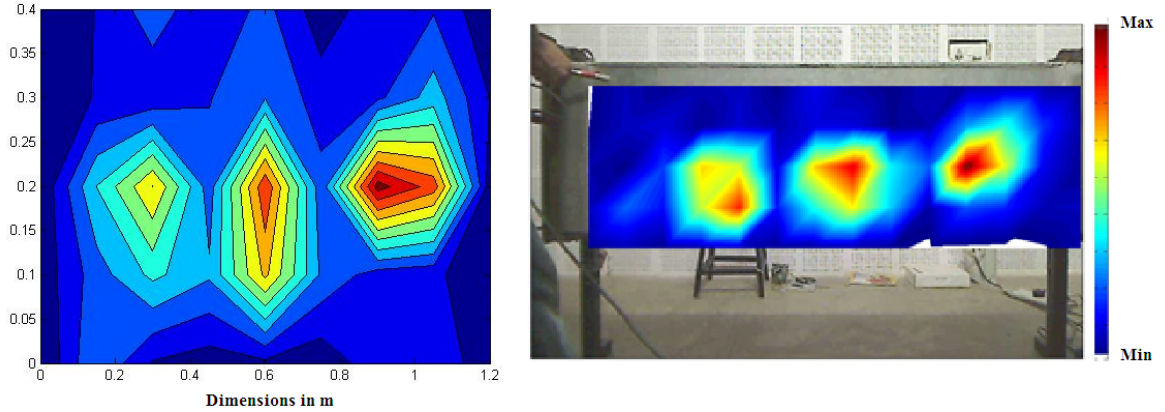

Figure 4.3: Comparison of PU probe with acclerometer data for displacement measurement

consistent, the magnitude has to be verified. PU probe using S&P was comparatively less time consuming and possess more accuracy than accelerometer-DAQ set up.

4.3.2   Sound Power Measurement using PP probe

By defining a control surface over the rectangular duct of sides 0.58m× 1.28m and 0.42× 1.28m scanning is done using PP probe. B&K intensity measurement kit was used to measure. Standard for measuring intensity was ISO 9614-2, a scanning based approach. Sound input signal chosen is random noise. Total sound power radiated from duct surface is given in fig. 4.5. Interested frequency range is 0-1000 Hz. The fig. 4.4 shows the experimental setup for measuring the sound power using PP probe over the control surface.
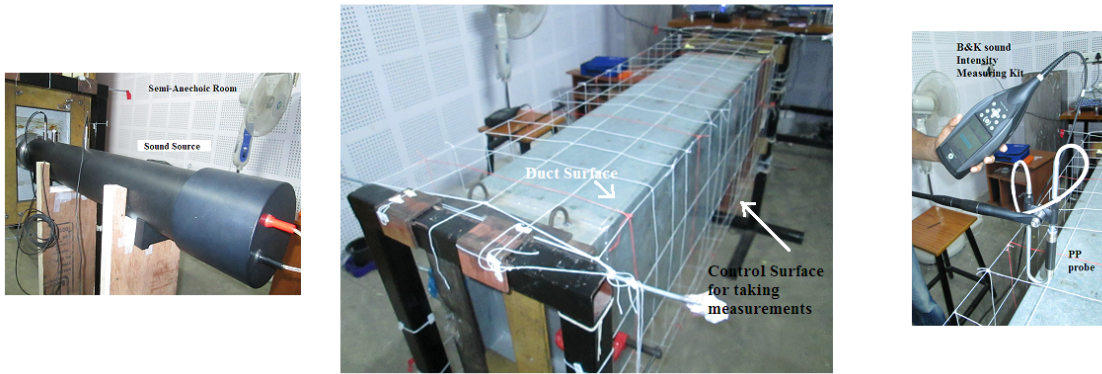
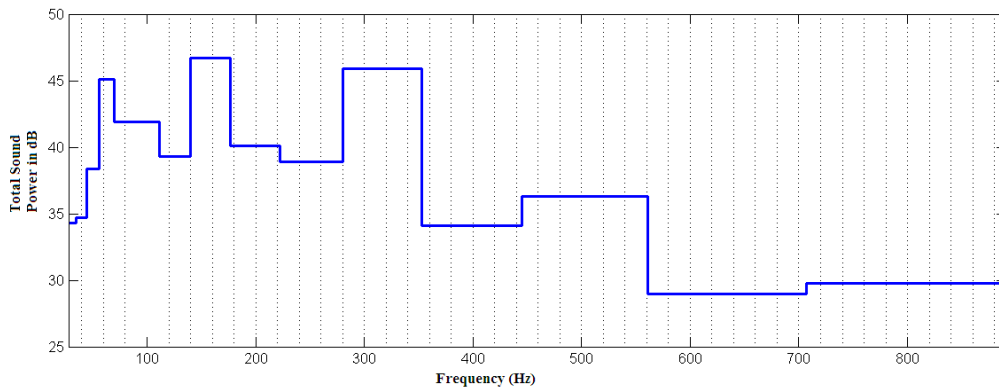Figure 4.4: Sound measurement set up using B&K sound intensity measuring kit

Figure 4.5: Total sound power measured using PP probe in $1/3^{rd}$ octave band frquencies

4.3.3 Sound Power Measurement using PU probe

Using Scan and Paint Technique, which uses PU-probe, plotted the sound power curves in dB for $1/3^{rd}$ octave band frequencies for each lateral surface of the rectangular duct (see figures 4.8 to 4.11). Test conditions were same to that of measurement using PP probe. Input sound signal is random noise. Note that the curve type chosen is line type. Scanning speed has to be consistent. Grid method was used to interpolate data over duct surface. Reactivity should be less than 7 dB to have an accuracy of $\pm$ 1 dB. Results are painted in colour scale over measured surface, as shown in fig. 4.7

Finally, all the power curves corresponding to each duct wall is summed up to get the total radiated sound power, shown in fig. 4.12
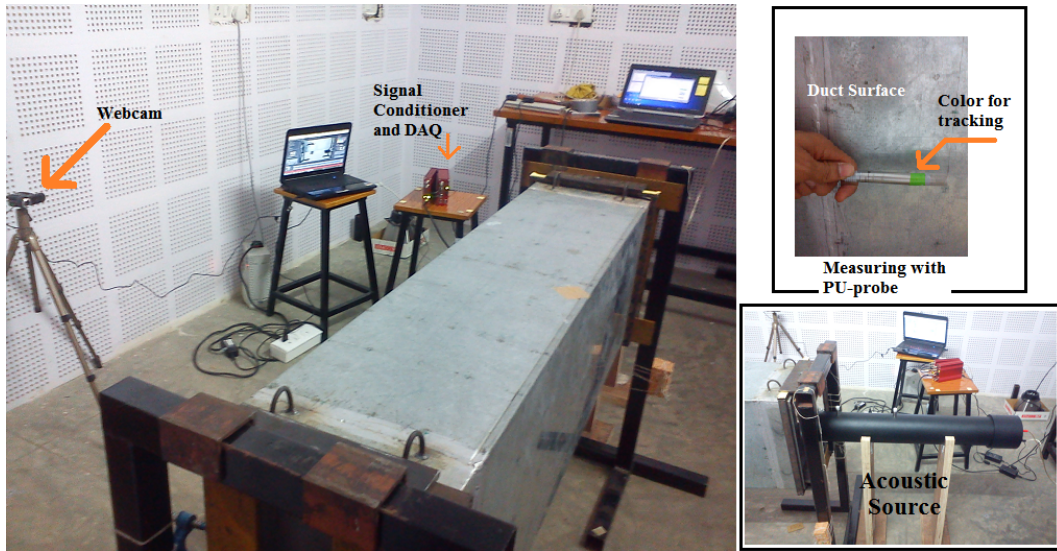
Figure 4.6: Sound power measurement set up using Scan and Paint

Figure 4.7: Generation of intensity colour plot after scanning duct surface
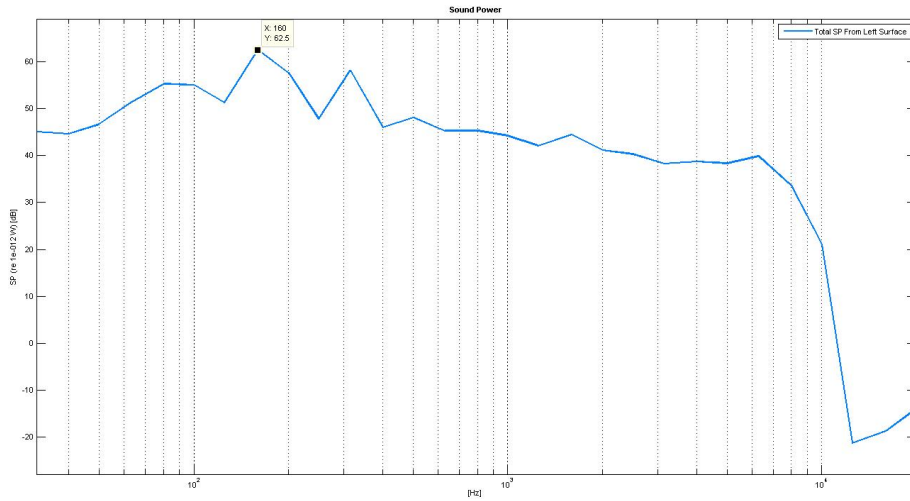
Figure 4.8: Sound power radiated from left surface
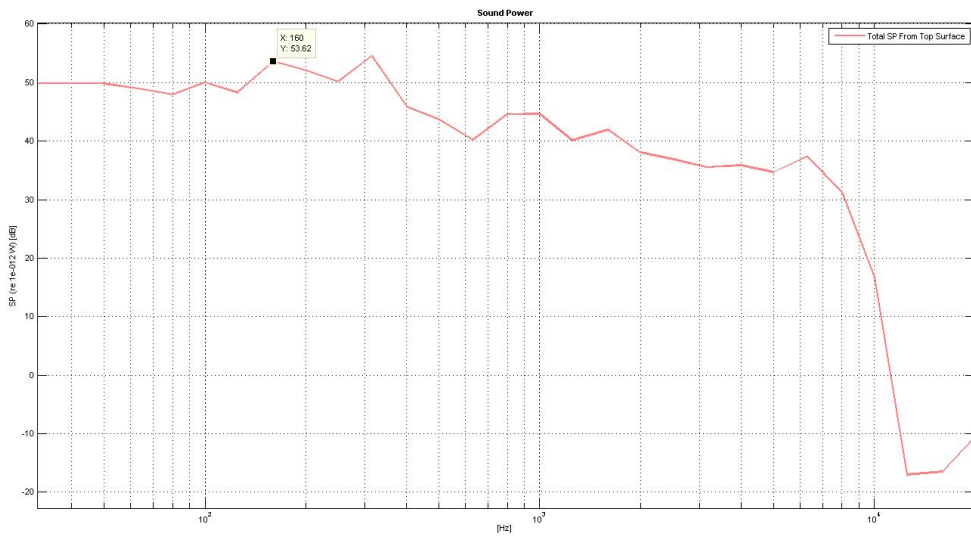

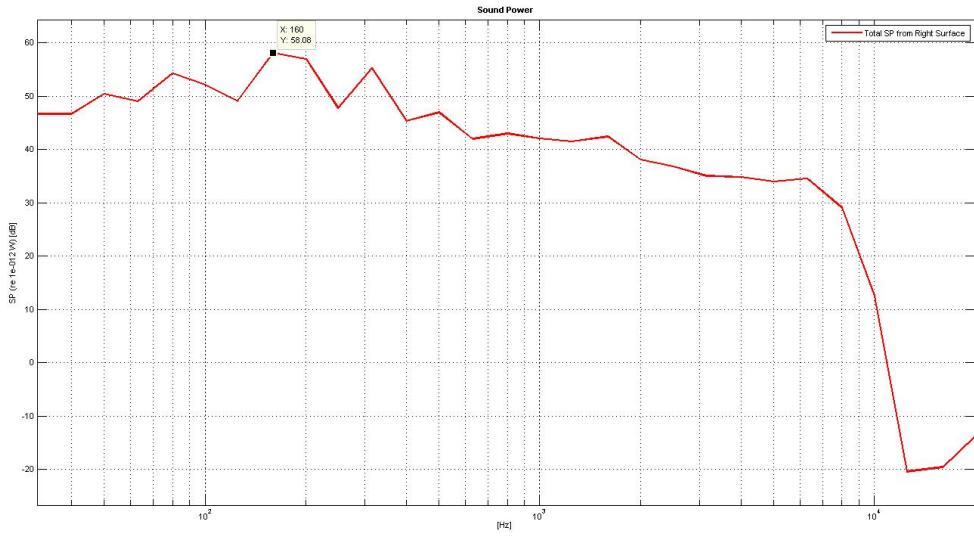Figure 4.9: Sound power radiated from top surface

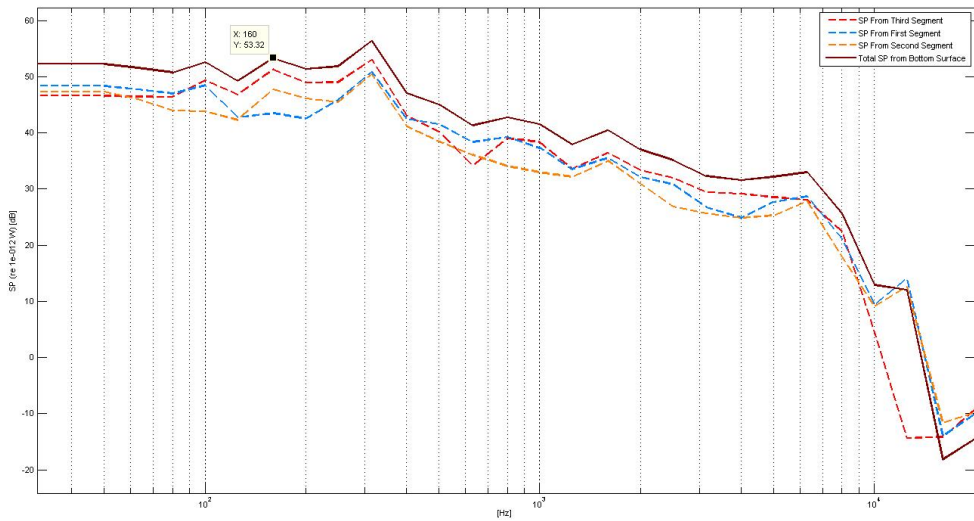Figure 4.10: Sound power radiated from right surface

Figure 4.11: Sound power radiated from bottom surface
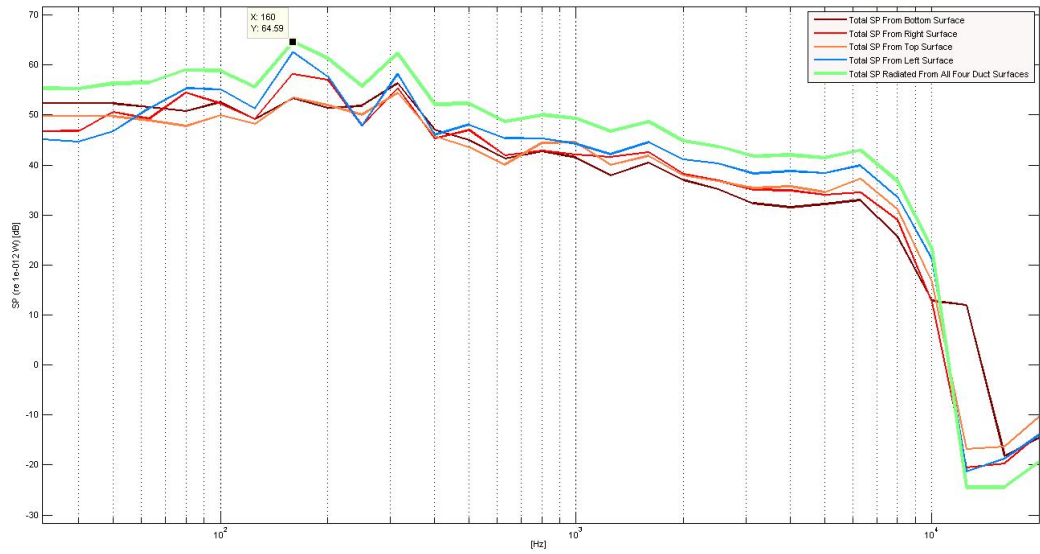
Figure 4.12: Total sound power radiated summing all surfaces

4.3.4   PU probe and PP probe measurement comparison

Both techniques was used to measure the sound power radiated for the same random noise input. But datas are not consistent with each other. Since both curves have same trend as shown in fig. 4.13, the possible cause of error would be improper calibration. To carry out calibration, measurements with both probes using a known sound source and same input sound power condition has to be done.

Figure 4.13: Total sound power radiation measured using PU an PP probes in $1/3^{rd}$ octave band frequencies

Chapter 5

Conclusion and Future Scope
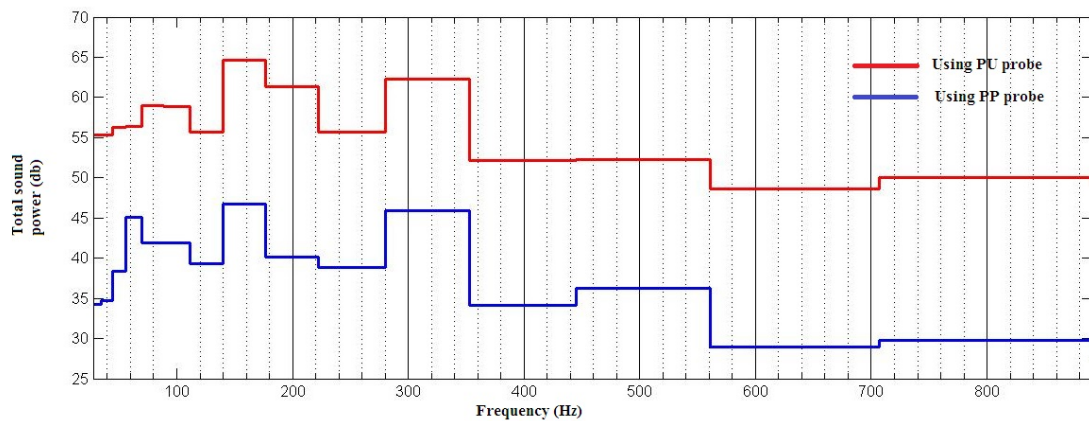
5.1 Conclusion

Various experimental techniques have been implemented to find the structural-acoustic coupling effects in rectangular duct and interior acoustic medium. As a first step to coupled analysis of these two subsystems, we have carried out the experimental modal analysis of the rectangular duct.

A prior study of EMA was conducted by taking 1D and 2D elements, like cantilever beam and ractangular plate. Modal Assurance criterion was successfully used as a tool for checking consistency of mode pairs of EMA and NMA. Also, studied effect of the boundary conditions, the numerical modelling gets difficult as practically implementing those ideal boundary conditions is difficult. Numerical Modal Analysis always serves as a guide for conducting EMA. The number of excitation locations, estimation of reference position on any non-nodal location and selection of frequency range of interest, hammer tip and accelerometer type are all decided from the initial NMA of the structure.

Modal density of the structure was high which made it cumbersome to extract every modes. Boundary conditions other than free-free makes it further difficult to model a structure numerically. Wrinkling of the duct due to welding, inorder to attach extended wall and end plates resulted in the deviation of duct from ideal conditions. Rotational stiffness of the duct edges were found to play a major role in numerical modelling, as fundemental frequency was able to capture by considering it. The role of extended wall and end plates have brought more uncertainty to the numerical structure.

Acoustic modes were found to contribute more to the sound power radiation of the duct, as maximum values of sound power are found to be closer to fundemental acous-

tic modal frequency from the sound power radiation curves measured.

Sound power radiation measurement techniques have been successfully implemented. Eventhough sound power radiation from duct surface using PP and PU was measured, datas were not consistent. Still, the datas had the same trend. Strongly beleived to be the fault of calibration.

For providing plane progressive sound waves, a cylidrical duct was attached to the source speaker. Sound input power was measured based on the assumption that sample, which is the duct here, will not disturb the source signal. But in practice, source itself is acting as a reactive muffler due to coupling phenomena. Sound input power was experimentally measured based on autospectral density of progressive pressure wave.

5.2   Future Scope

EMA of flexible rectangular ducts, with different aspaect ratios can be conducted. Thereby, extraction of modal parameters for thin shell structures, having high modal densities can be studied. Also, the severity of effects caused by incorporating extended walls and end plates are possible to analyse. Empirical study of joints as well as edges for different wall thickness, should be conducted to obtain its rotational stiffness constants.

Instead of giving simply supported condition and provision for mounting speaker seperately, both can be arranged in a single unit. That is, a speaker which is supported externally and it's outer wall supporting the rectangular duct. Other end can be straight away given a simple support. As it is rectangular geometry, this would be a challenge. Obviously numerical modelling would be much easier.

Sound input power measurement methodology implmented here have to be revisited considering the interaction of noise generated by the duct, with the source sound.

The coupling phenomena using numerical simulation could be validated with experimental results. Finally, the analytical model[4], representing rectangular duct as an unfolded plate with creases and joints replaced with linear and rotational springs, respectively, has to be proved experimentally.

References

[1] A. Cummings. Low frequency acoustic transmission through the walls of rectangular ducts. *Journal of Sound and Vibration* 61, (1978) 327 – 345.

[2] R. Astley and A. Cummings. A finite element scheme for acoustic transmission through the walls of rectangular ducts: Comparison with experiment. *Journal of Sound and Vibration* 92, (1984) 387 – 409.

[3] A. Cummings. Sound transmission through duct walls. *Journal of Sound and Vibration* 239, (2001) 731 – 765.

[4] B.Venkatesham and M. Munjal. Analytical prediction of break-out noise from a reactive rectangular plenum with four flexible walls. *Journal of the Acoustic Society of America* 128, 2010.

[5] T. R. Lin and J. Pan. Vibration characteristics of a box-type structure. *Journal of Vibration and Acoustics* 131, (2009) 9.

[6] V. L. ALLEY and S. A. LEADBETTER. Prediction and Measurement of natural vibrations of multistage launch vehicles. *AIAA* 1, (1963) 374–379.

[7] S. Farshidianfar. Vibration analysis of long cylindrical shells using acoustical excitation. *Journal of Sound and Vibration* 330, (2011) 33813399.

[8] M. Pastor, M. Binda, and T. Hararik. Modal Assurance Criterion. *Procedia Engineering* 48, (2012) 543 – 548.

[9] M. Munjal. Acoustics of Ducts and Mufflers. 2nd edition. 2014.

[10] M. H. R. Brian J. Schwarz. Experimental Modal Analysis. Vibrant Technology, Inc., Jamestown, California 95327, 1999.

[11] R. Praveena. Thesis, Sound Radiation Characteristics of Rectangular Ducts . IIT Hyderabad, 2013.

[12] Manual Scan and Paint ver 2.1, 2014.

[13] m+p international. SO analyser ver 2.1, Freundallee 17 30173 Hannover Germany,October 2011.

[14] ANSYS 13 User guide, ANSYS,Inc.

[15] LMS Virtual Lab Rev 11, Users Manual.